2024 IEEE International Conference on Robotics and Automation (ICRA 2024)
May 13-17, 2024. Yokohama, Japan

Intraoperatively Iterative Hough Transform Based In-plane Hybrid Control of Arterial Robotic Ultrasound for Magnetic Catheterization

Zhengyang Li, *Student Member, IEEE*, Magejiang Yeerbulati, and Qingsong Xu*, *Senior Member, IEEE*

***Abstract*— This paper presents an intraoperatively iterative Hough transform (IHT) based in-plane hybrid control of extracorporeal ultrasound (US) guided magnetic catheterization for arterial intervention. One uniqueness lies in that both control and tracking of the arterial robotic ultrasound end-effector have been implemented to improve performance. Firstly, the magnetic catheter model and hybrid visual/force servoing control scheme of the extracorporeal ultrasound-integrated tracking arm (EUTA) are derived based on the interaction Jacobian matrix and impedance modeling. Meanwhile, we implement a tracking method of in-plane ultrasound catheter's tip and detection of vascular boundaries utilizing intensity-level iterative Hough-transform with Iterative End-Ponit Fitting (IEPF). The effectiveness of the proposed control and tracking method has been verified by conducting *in vitro* experimental studies for catheter steering of a soft tissue-imitating phantom. Results show that an average steering error of 0.56 mm and signal-to-noise-ratio (SNR) of 12.2 are obtained for the ultrasound imaging at high synchronization along with a low target lost rate (15.8%) and constant-force tracking (2.50±1.02 N).**

I. Introduction

Robotic-assisted ultrasound (RUS) is a promising technology that can be utilized to conduct diagnostic imaging and surgical tracking [1]. For cardiovascular surgery, X-ray imaging-based digital subtraction angiography (DSA) is the dominant imaging modality to detect the region of interest (ROI) [2]. However, long-term radiation exposure would cause damage to both the patient and the surgeon [3]. RUS is a radiation-free solution that could detect the arterial region of interest [4], and also provide visual feedback to close the control loop of surgical robots [5].

Magnetic catheterization (MC) [6]–[9] is an autonomous robotic surgical solution, which exhibits great potential for minimally invasive surgery (MIS) applications, such as arterial intervention [10], cardiac ablation [11], and atherectomy [12]. Autonomous magnetic catheterization relies on the visual feedback information provided by intraoperative medical imaging [13]. Recently, Sikorski et al. [14] have proposed a template-based magnetic catheter shape reconstruction method using out-of-plane repetitive ultrasound scanning. However, the above work did not utilize the visual feature information to drive the robotic ultrasound motion.

This work was supported in part by the National Natural Science Foundation of China under Grant 52175556, the Macao Science and Technology Development Fund under Grant 0004/2022/AKP, and 0102/2022/A2, the University of Macau under Grant MYRG2022-00068-FST and MYRG-CRG2022-00004-FST-ICI, and the Guangdong Basic and Applied Basic Research Foundation under Grant 2023A1515011178.

The authors are with the Department of Electromechanical Engineering, Faculty of Science and Technology, University of Macau, Avenida da Universidade, Taipa, Macau, China qsxu@um.edu.mo

*Corresponding author: Q. Xu (Tel.: +853-88224278).

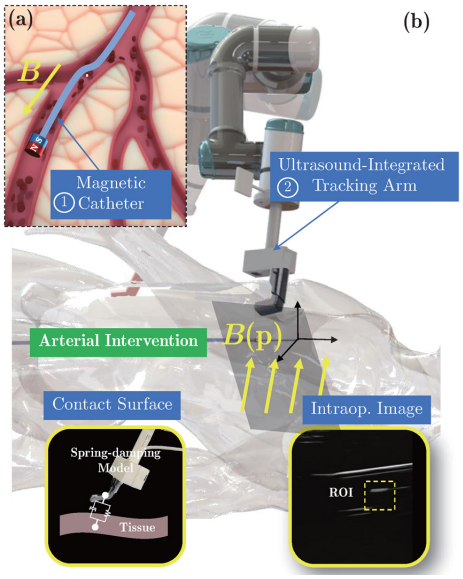

Fig. 1. Illustration of the in-plane ultrasound-guided intervention of a magnetic catheter. (a) The multi-vessel arterial intervention scenario using the magnetic catheter ①. (b) The EUTA ② is conducting the intraoperative ultrasound scanning with a hybrid visual/force controller with impedance modeling.

To realize visual servoing control of the RUS intraoperatively, some previous work has been conducted via instrument tracking and localization using RUS in the literature [1]. Nevertheless, unlike flexible needle steering [15], the synchronization of the robotic ultrasound probe and magnetic catheter's tip is crucial for autonomous endovascular intervention guided by RUS. The ultrasound probe should keep moving to track both the arterial routes and the catheter's tip, while maintaining contact with the patient's body. To realize a stable scanning performance, a hybrid visual/force controller is required to implement the robotic-assisted arterial magnetic catheterization with ultrasound guidance.

To acquire feature information and provide the velocity of the instrument movement, the catheter's motion should be detected inside the US image plane [16]. General model-fitting methods include random sample consensus (RANSAC), Hough transform (HT) [17], and parallel integral projection (PIP) [18]. Recently, Yang et al. [19] proposed a RANSAC-based tracking method to track a magnetic guidewire's tip. However, regarding the tubular scenario inside the endovascular environment, there are many line shapes within the image domain (e.g., vascular boundaries, tip magnet, and catheter's tube body), where RANSAC is not suitable for

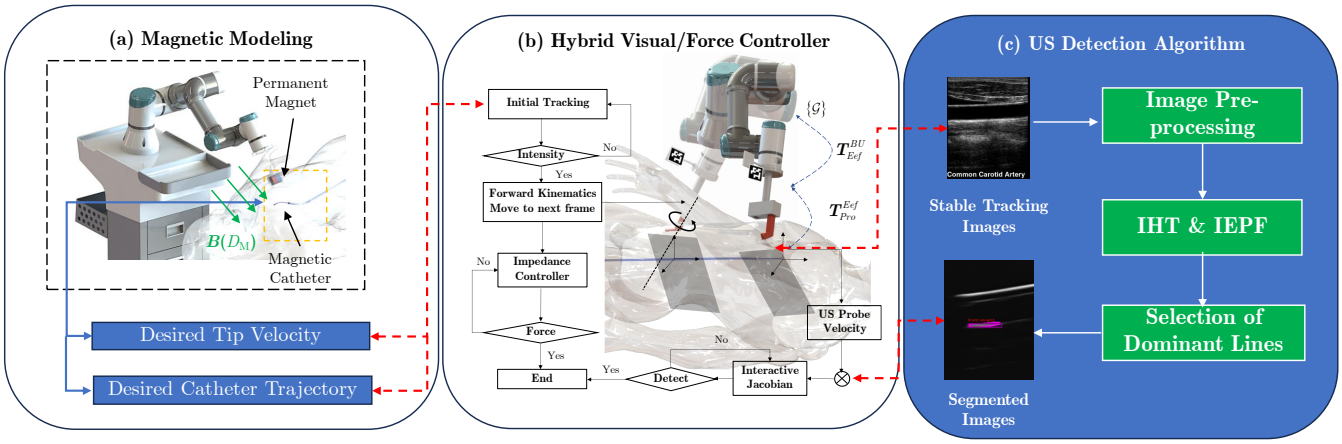

Fig. 2. The control diagram of the proposed hybrid visual/force controller. (a) The modeling of the magnetic catheter actuated by the external magnetic field. A cylinder permanent magnet is integrated into the end-effector of a 6-DOF manipulator. (b) The hybrid visual/force controller for EUTA. (c) The detection algorithm using the IHT and IEPF to detect the catheter's tip.

individual line detection. Alternatively, Hough-transform (HT) is a feasible method for the line-detection with multiple line existence and has been applied to the arterial US detection [20]. However, few work on control and tracking of the arterial robotic ultrasound end-effector has been conducted in the literature.

The main contributions of this work are listed below. Firstly, we propose a hybrid visual/force feedback controller for an arterial robotic ultrasound system. Secondly, we propose a novel intensity-level iterative Hough transform-based in-plane magnetic catheter motion detection method for arterial intervention. Its effectiveness has been verified by conducting extensive *in vitro* experimental tests. In the following sections, the magnetic catheter modeling and hybrid visual/force controller are introduced in Section II. Section III shows an interactive Hough transform and IEPF-based magnetic catheter's tip during the intraoperative ultrasound tracking. We validate the proposed control and tracking method and present the results in Section IV. Section V summarizes the paper.

II. Hybrid Visual/Force-Based Controller for Arterial Robotic Ultrasound

A. Modeling of Magnetic Catheterization

The targeted surgical scenario for a robotic-assisted catheterization is shown in Fig. 1. The magnetic catheter ① is steered inside the multi-vessel environment driven by an external magnetic field $\mathbf{B}(p)$. The extracorporeal ultrasound system with an ultrasound probe is integrated into a six-degree-of-freedom (DOF) robotic arm ② (model: UR3 e-Series, from Universal Robots, Odense, Denmark). The mobile robotic ultrasound is deployed over the patient's body with the ultrasound probe contacting the skin surface. The surgeons could receive the ultrasound imaging sequences on the main computer streaming from the ultrasound scanning to localize the catheter's tip. The cathter's kinematic motion is modeled using the piecewise constant curvature (PCC) theory [21]. Concerning a magnetic catheter, the main deflection of the catheter's tip is induced by an external permanent magnet, which is integrated to the end-effector of a robotic arm, as shown in Fig. 2(a). If the magnetic component is represented by its dipole moment $\mathbf{m}_E \in \mathbb{R}^3$, the exerted magnetic wrench $\mathbf{W}_m \in \mathbb{R}^6$ by the external magnetic field can be derived below.

$$\mathbf{W}_m = \begin{bmatrix} \mathbf{F}_m \\ \mathbf{T}_m \end{bmatrix} = \begin{bmatrix} \nabla(\mathbf{m}_E{}^T \mathbf{B}(p)) \\ S(\mathbf{m}_E)\mathbf{B}(p) \end{bmatrix} \tag{1}$$

where $\mathbf{F}_m$ and $\mathbf{T}_m$ are the magnetic forces and torques. The matrix operator S represents its skew-symmetric form, and $\mathbf{B}(p)$ is the magnetic field, which can be defined as:

$$\mathbf{B}(D_M) = \left(\frac{\mu_0}{4\pi \|p\|^3} \left(3\hat{D}_M \hat{D}_M^T - \mathbf{I}_3 \right) \right) \mathbf{m}_E \tag{2}$$

where $p = D_M$ is the distance from the measurement position to the centerline of the permanent magnet, $\mathbf{I}_3$ is the identity matrix, and μ_0 denotes the permeability of free space. The tip velocity $\dot{P}_c \in \mathbb{R}^3$ and desired trajectory $P_c \in \mathbb{R}^3$ could be used as reference input of the hybrid visual/force controller for the EUTA.

B. Hybrid Visual/Force Servoing Control of the Robotic Ultrasound

The overall hybrid visual/force control scheme is shown in Fig. 2(b). We set the intensity of the US image frame as $\mathbf{s} = (I_{1,1}, \ldots, I_{u,v}, \ldots, I_{M,N})$, where u and v are the coordinates in the image frame, and M and N are the maximum voxel number of a single image. The relationship between the intensity inside the image plane and the ultrasound probe could be defined as follows.

$$\mathbf{P}_u = -k_d \widehat{\mathbf{J}}_s^{+} \left(\mathbf{s}(t + \Delta t) - \mathbf{s}^* \right) \tag{3}$$

where $\mathbf{P}_u$ is the velocity of the US probe. $\widehat{\mathbf{J}}_s^{+}$ is the pseudo-inverse of the US interactive Jacobian matrix [22], and k_d is the velocity control gain. Meanwhile, to modulate the contact force between the ultrasound probe and the patient,

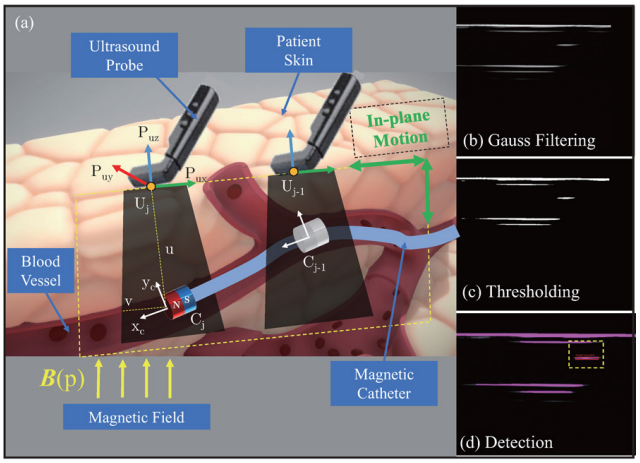

Fig. 3. (a) Illustration of the in-plane ultrasound-guided intervention of a magnetic catheter. (b) Gauss filter of initial raw US image. (c) Image after thresholding operation. (d) Catheter's tip detection.

we implement an impedance controller for the EUTA as follows.

$$\tau_{\mathbf{u}} = \mathbf{J}_u^T[\mathbf{K}_{uf}\left({}^{des}\mathbf{P}_u - \mathbf{P}_u\right) + \mathbf{F}_u] + \hat{\mathbf{H}}\left(\mathbf{q}_u, \dot{\mathbf{q}}_u, \ddot{\mathbf{q}}_u\right) \quad (4)$$

where $\tau_u \in \mathbb{R}^{6\times 1}$ is the target torque for all joints of EUTA, $\mathbf{K}_{uf}$ is the stiffness gain, $\mathbf{F}_u$ is the desired contact force, and $\hat{\mathbf{H}}\left(\mathbf{q}_u, \dot{\mathbf{q}}_u, \ddot{\mathbf{q}}_u\right)$ is the Coriolis force and centrifugal term of the EUTA.

C. Transformation of Mobile Ultrasound System

To utilize the US image frame to control the EUTA (see Fig. 2(a)), we can calculate the homogenous transform from the image plane to EUTA base ${}^{BU}\mathbf{T}_{US}$ as follows.

$${}^{BU}\mathbf{T}_{US} = {}^{BU}\mathbf{T}_{Eef} \cdot {}^{Eef}\mathbf{T}_{Pro} \cdot {}^{Pro}\mathbf{T}_{US} \quad (5)$$

where ${}^{BU}\mathbf{T}_{Eef}$ denotes the transformation from the end-effector to EUTA base, and ${}^{Eef}\mathbf{T}_{Pro}$ describes the transformation from the end-effector to the ultrasound probe. The transformation from the US image frame to ultrasound probe frame ${}^{Pro}\mathbf{T}_{US}$ can be derived below.

$${}^{Pro}\mathbf{T}_{US} = \begin{bmatrix} 0 & 0 & -1 & 0 \\ -\frac{L_p}{W_{us}} & 0 & 0 & \frac{L_p}{2} \\ 0 & \frac{D}{H_{us}} & 0 & \varepsilon_0 \\ 0 & 0 & 0 & 1 \end{bmatrix} \quad (6)$$

where L_p, W_{us}, H_{us}, and ε_0 are geometric parameters of the ultrasound probe. The kinematic model of the end-effector of permanent magnet and EUTA can be expressed in the base coordinate frame as ${}^{BU}\mathbf{T}_{Eef} = {}^{B}\mathbf{T}_{Eef}\left(d_i, \theta_i, L_i, \alpha_i\right)\mathbf{P}_B$, where d_i, L_i, θ_i, and α_i are Denavit-Hartenberg (DH) parameters [23].

III. Iterative Hough Transform Based In-plane Catheter Detection under Tubular Environment

The detection of the catheter's motion inside the US imaging plane could provide clear feedback to the surgeon regarding the surgical ROI and instrument localization. The general workflow of the detection algorithm is shown in Fig. 2(c).

Algorithm 1 Iterative Hough-Transform and IEPF Algorithm

Require: Input US image frames $U_j, j \in \mathbf{s}$; Minimum vote count $n_{\min}$;

Ensure: Tracked real catheter tip positions $\mathbf{P}_c^t \in \mathbb{R}^3$; Tracked vascular boundaries line $\mathbf{P}_v^t \in \mathbb{R}^3$;

$\mathbf{U}_j^{Gau} \leftarrow Gauss\_Filter\left(U_j\right)$; ▷ Image Pre-process: Denoising

$\mathbf{U}_j^{Thr} \leftarrow Threshold\left(U_j\right)$; ▷ Image Pre-process: Thresholding;

while $U\left(u,v\right) \in U\left(M,N\right)$ **do** ▷ Initial Tracking

  vote_count n = get_vote_count(u, v);

  if $vote\_count > threshold$ **then**

    Search for the maximum of $\mathbf{H}$ at position; ▷ Iterative Hough Transform

    if $Lines[i].length > threshold$ **then**

      Find_curve_fitting_polygon ;

    end if

  end if

end while

for $Lines(i) < Line(max)$ **do** ▷ IEPF

  if $Lines[i].length > threshold$ **then**

    Calculate_Euclidean_Dist ;

  else

    $Lines[i] \leftarrow DetectedCatheter$; ▷ Catheter's tip detected

  end if

end for

A. Denoising and Thresholding Operation

The in-plane sequential US tracking of the magnetic catheter inside the tubular environment is shown in Fig. 3(a). The intensity $I_{u,v}\left(t\right)$ of j-th frame U_j in the B-mode image (acquired by the US probe at the time t) corresponds to j-th catheter's tip location points $C_j \in \mathbf{C}_n\left(n = 1, 2, \ldots\right)$. Gauss filtering is utilized to denoise the raw US data set. Then, a set of voxels with coordinates and intensities $I\left(X\right)$ is split by thresholding into two disjoint sets: $I_c\left(x\right)$ (tip's voxels) and $I_b\left(x\right)$ (background voxels) as follows.

$$I_c\left(x\right) = \{I_c\left(x_i\right) \in I\left(X\right) : I\left(x\right) > I_{Th}\} \quad (7)$$

$$I_b\left(x\right) = I\left(X\right) \setminus I_c\left(x\right) \quad (8)$$

where I_{Th} is the intensity of thresholding. The image pre-processing results are shown in Fig. 3(b)–(c).

B. Iterative Hough Transform

The iterative Hough transform discretizes the parameter space of line and randomly samples the pairs of voxels after certain thresholding, increasing the appropriate accumulator bin [17]. Let $C_j \in \mathbf{C}_n\left(n = 1, 2, \ldots\right)$ be the set of points of interest in the US image space, forming the set of curve line $\mathbf{L}$ by adjacent points. The corresponding Hough transform $\Gamma_C\left(L\right)$ of the US images is defined as:

$$\Gamma_C\left(L\right) : M(C_x - N)^3 - A\left(C_x - N\right) - B - C_y^2 = 0 \quad (9)$$

where M and N are the width and depth of the ROI in the 2D ultrasound domain. A and B are unset parameters. The

accumulator matrix H_n is given below.

$$H_n = H_{n_1,n_2,\cdots,n_t} := \#\left\{C_j | \Gamma_{C_j}(L) \cap \mathbf{C}_n \neq \varnothing\right\} \quad (10)$$

which is computed by the means of iterative process as follows.

$$H_{\mathbf{n}}^{j} = \begin{cases} H_{\mathbf{n}}^{(j-1)} + 1 \text{ if } \Gamma_{C_j}(L) \cap \mathbf{C}_n \neq \varnothing \\ H_{\mathbf{n}}^{(j-1)} \text{ if } \Gamma_{C_j}(L) \cap \mathbf{C}_n = \varnothing \end{cases} \quad (11)$$

The iteration continues until the line set $\mathbf{L}$ best approximates the set of points C_j in the US image.

At the same time, the Iterative End-Point Fit (IEPF) algorithm uses a distance threshold to generate the segmentation [24]. Let the distance $Dist(i)$ be the distance of the i-th estimated point and the original pixel point around the catheter's tip. Then, the simultaneous Euclidean distance $Dist_E$ could be expressed as:

$$Dist(i) = \sqrt{(u_i - u'_i)^2 + (v_i - v'_i)^2} \quad (12)$$

$$Dist_E = \frac{1}{n}\sum_{i=1}^{n} Dist(i). \quad (13)$$

The similarity between the sequential US images is evaluated using the normalized cross correlation (NCC) criterion. The best estimation means that the NCC value V is maximal, which could be expressed below [25].

$$V = \frac{\sum_{u=0}^{M}\sum_{v=0}^{N}\left(I_{u,v}(x) - \bar{I}\right)\left(T_{u,v}(x) - \bar{T}\right)}{\sqrt{\sum_{u=0}^{M}\sum_{v=0}^{N}\left(I_{u,v}(x) - \bar{I}\right)^2}\sqrt{\sum_{u=0}^{M}\sum_{v=0}^{N}\left(T_{u,v}(x) - \bar{T}\right)^2}} \quad (14)$$

where $T_{u,v}$ is the previous image as the template. $\bar{I}$ and $\bar{T}$ represent the mean value of the US image intensity. The detailed process of the catheter's tip detection is listed in **Algorithm 1**. The detected catheter is shown in Fig. 3(d).

IV. Experimental Validation and Results

In this section, the *in vitro* experiments have been carried out to assess the pivotal performance of the proposed method on a soft gelatinous phantom, including magnetic catheter's intervention precision, hybrid visual/force control performance, and ultrasound tracking accuracy.

A. Experimental Setup

The experimental setup is shown in Fig. 4. The robotic ultrasound system was set up on a test platform to simulate the setting of an operating room. An external permanent mobile magnet (⌀30 mm × 30 mm) is mounted on the end-effector of a 6-DOF robotic arm (model: UR5 e-Series, from Universal Robots, Odense, Denmark). A stereo camera (model: ZED 2i, from Stereolabs, CA, USA) is harnessed to calibrate the local frames of each robotic arm to the global frame by ArUco markers. The effectiveness of the proposed controller is evaluated by a custom-made soft and transparent gelatin-agar phantom (with 1:1 AB pattern) molding. It is obtained from an anthropomorphic thoracoabdominal training model with a multi-vessel phantom model embedded imitating the

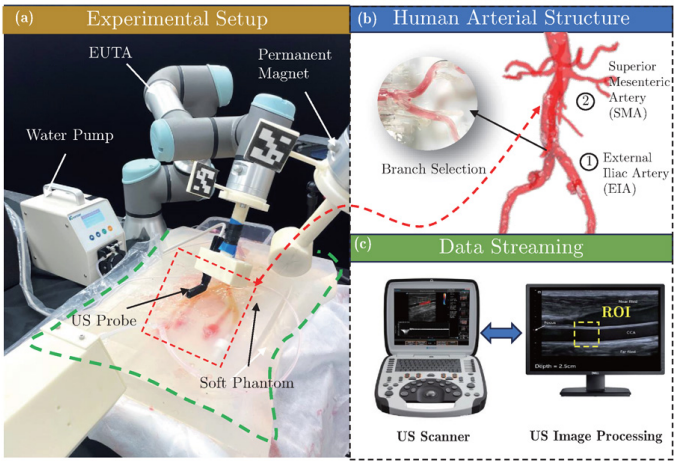

Fig. 4. The experimental setup for the magnetic catheterization with ultrasound guidance.

superior mesenteric artery (SMA) and external iliac artery (EIA), as shown in Fig. 4(b) (size: 450 × 350 × 50 mm^3, with branch inner diameter ranging from 0.5 to 16 mm). The blood fluid is also imitated via an external water pump with a fluid velocity of 35 mL/min. The control frequency of the inner control is set as 125 Hz.

The EUTA is mounted with an ultrasound probe (model: 16HL7, frequency: 7–16 MHz) connected to an ultrasound scanner (model: uSmart 3300, Terason, MA, USA) with a depth setting of 7.0 cm. The contact forces are measured by the joint current provided by Universal Robots. The catheter's tip is intraoperatively tracked using a detection algorithm during the robotic US scanning with a probe frequency (15 MHz) and dynamic range (45 dB). The ultrasound tracking sequences are streaming to the host computer to run the imaging processing algorithm (see Fig. 4(c)). In addition, an off-the-shelf Intel NUC is powered by an Intel Core i7-11700 @2.60 GHz and 32 GB of RAM.

B. Ultrasound-Guided Intervention on an Anthropomorphic Phantom

To show the performance of the proposed method, we conducted an experiment to steer the magnetic catheter through a narrow channel within a human arterial-like phantom. The whole experimental process and detection performance are shown in Fig. 5.

As shown in Fig. 5(a), once the initial tracking is accomplished as the intensity of the vascular boundaries, and the catheter's tip I_{Th} reaches the threshold value, the catheter's tip and the arterial boundaries are segmented and labeled into different colors relative to the background. When the US images are stable, the magnetic catheter starts to steer forward. The iterative Hough-transform and the IEPF algorithm are applied during the procedure. Meanwhile, the hybrid visual/force servoing control method is utilized to drive the EUTA motion during the scanning. The US imaging frame should move at the same velocity as the catheter's tip with an average scanner velocity 10.20±0.65 mm/s.

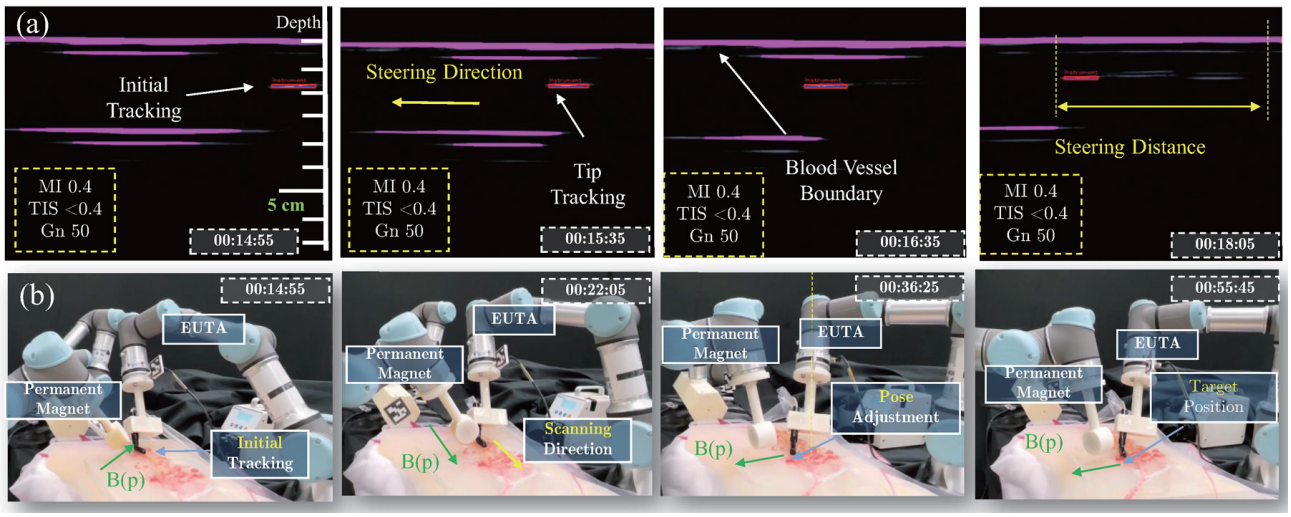

Fig. 5. Hybrid visual/force-controlled ultrasound tracking results of the multi-arm robotic system with *in vitro* soft anthropomorphic phantom. (a) The real-time tip tracking (red rectangle) and arterial boundaries (purple line) provided by the ultrasound scanner at different time instants of 14.55 s, 15.35 s, 16.35 s, and 18.05 s under ultrasound parameters of thermal index score (TIS) < 0.4, mechanical index (MI) of 0.4, gain settings (Gn) of 50, frequency of 7–16 MHz, and depth of 2 cm. (b) Performance test result of the hybrid visual/force control applied to the multi-arm robotic system.

Simultaneously, the US probe should ensure the trajectory following of the arterial route when the magnetic catheter arrives at a branch selection (see Fig. 4(b)). The movement snapshots of the multi-arm and tracking system are shown in Fig. 5(b). The experimental results show that, with the hybrid visual/force controller, the proposed system could autonomously navigate the magnetic catheter to reach the target ROI under a magnetic field generated by the permanent magnet, while simultaneously tracking the catheter's tip with EUTA to form a closed-loop control. The tracking errors in the Cartesian space for the EUTA are $[0.68\,\mathrm{mm}, 0.57\,\mathrm{rad}]$ [see Fig. 6(a)]. The root-mean-square error (RMSE) of the catheter's tip is calculated as 0.56 mm. The impedance control method (as proposed in Section II) is validated using the ultrasound scanner contacting the anthropomorphic tissue phantom with a constant force. The stiffness matrix is set as $\mathbf{K}_{uf} = \mathrm{diag}\,[3000, 1000, 300, 20, 20, 20]$. The corresponding force tracking results are shown in Fig. 6(c). We can see that the contact forces are stabilized around 2.50 N with an average error of 1.02 N relative to the ground truth in z-axis direction.

The SNR compares the desired signal to the noisy signal. A higher value of the ratio indicates less prominent of the noise. It is expressed in decibels (dB) as follows.

$$\mathrm{MSE} = \frac{1}{NV^2} \sum_{i,j=1}^{NV-1} (X_{i,j} - Y_{i,j})^2 \tag{15}$$

$$\mathrm{SNR} = 10\log_{10} \frac{\sigma^2}{\sigma_e^2} \tag{16}$$

where σ^2 and σ_e^2 are the variance of the original image and variance of the error, respectively. The computed MSE and SNR are shown in Table I.

The steering results indicate that the proposed multi-arm robotic system could successfully navigate and track the

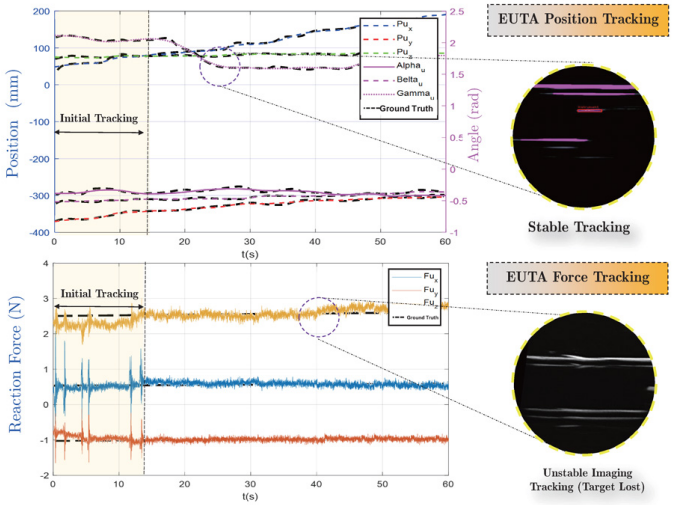

Fig. 6. The performance test results of the hybrid visual/force controller to navigate the magnetic catheter.

catheter's tip toward the target position. The validity of the proposed detection technique is investigated by comparing the area corresponding to the autonomously defined catheter's tip and vascular boundaries. The sensitivity (SE), specificity (SP), and accuracy (AC) are calculated as follows.

$$SE = TP/\left(TP + FN\right) \tag{17}$$

$$SP = TN/\left(TN + FP\right) \tag{18}$$

$$AC = \left(TP + TN\right)/NV \tag{19}$$

where NV is the total number of voxels in the US images and the corresponding results are shown in Table I. The rate of target loss of the catheter's tip during the scanning is around 15.8% (see Fig. 6(b)).

TABLE I

PERFORMANCE OF THE HYBRID VISUAL/FORCE CONTROLLER

	Specification	Value	Unit
Tracking Performance	Sensitivity (SE)	0.89±0.18	-
	Specificity (SP)	0.99±0.26	-
	Accuracy (AC)	0.97±0.22	-
	Signal-to-Noise Ratio (SNR)	12.2±0.24	-
	Mean-Square-Error (MSE)	51.2±1.22	-
Control Performance	Steering Error	0.56±0.16	mm
	Force Error	2.50±1.02	N

V. CONCLUSION

In this paper, we propose an intraoperatively iterative Hough-transform based hybrid control method for magnetic catheterization under in-plane ultrasound guidance for the first time. The magnetic catheter modeling is conducted, while a hybrid visual/force control scheme is proposed for achieving the steering of magnetic catheter by controlling the permanent magnet and EUTA at the same time. Meanwhile, an iterative Hough transform-based tracking for the region of interest is proposed. The detection algorithm adopts a Gauss filter for denoising and a thresholding method for the image pre-processing. An iterative end-point fitting method is utilized to create a polygon along with the catheter's tip motion. Moreover, *in vitro* magnetic catheter steering experiments are performed on an arterial-like soft tissue-imitating phantom. The success validation of the proposed magnetic robot catheterization system is performed on a silica-made anthropomorphic phantom under ultrasound tracking (mean error of 0.56 mm) and constant force tracking (2.50±1.02 N). The catheter's tip and vascular boundaries are successfully detected inside the US image domain. In future work, we will further enhance the method by applying shape sensing technology to detect the real-time shape configuration in the endovascular steering.

REFERENCES

[1] P. Chatelain, A. Krupa, and N. Navab, "3D ultrasound-guided robotic steering of a flexible needle via visual servoing," in *Proc. of 2015 IEEE Int. Conf. on Robotics and Automation (ICRA)*, pp. 2250–2255, 2015.

[2] R. Stein, I. Hriljac, J. L. Halperin, S. M. Gustavson, V. Teodorescu, and J. W. Olin, "Limitation of the resting ankle-brachial index in symptomatic patients with peripheral arterial disease," *Vascular Medicine*, vol. 11, no. 1, pp. 29–33, 2006.

[3] D. R. Mangels, J. Giri, J. Hirshfeld, and R. L. Wilensky, "Robotic-assisted percutaneous coronary intervention," *Catheterization and Cardiovascular Interventions*, vol. 90, no. 6, pp. 948–955, 2017.

[4] M. Chen, Y. Huang, J. Chen, T. Zhou, J. Chen, and H. Liu, "Fully robotized 3D ultrasound image acquisition for artery," in *Proc. of 2023 IEEE Int. Conf. on Robotics and Automation (ICRA)*, pp. 2690–2696, 2023.

[5] S. Pane, G. Faoro, E. Sinibaldi, V. Iacovacci, and A. Menciassi, "Ultrasound acoustic phase analysis enables robotic visual-servoing of magnetic microrobots," *IEEE Transactions on Robotics*, vol. 38, no. 3, pp. 1571–1582, 2022.

[6] Y. Kim, E. Genevriere, P. Harker, J. Choe, M. Balicki, R. W. Regenhardt, J. E. Vranic, A. A. Dmytriw, A. B. Patel, and X. Zhao, "Telerobotic neurovascular interventions with magnetic manipulation," *Science Robotics*, vol. 7, no. 65, p. eabg9907, 2022.

[7] M. F. Phelan III, M. E. Tiryaki, J. Lazovic, H. Gilbert, and M. Sitti, "Heat-mitigated design and lorentz force-based steering of an mri-driven microcatheter toward minimally invasive surgery," *Advanced Science*, vol. 9, no. 10, p. 2105352, 2022.

[8] Z. Li and Q. Xu, "Design and steering control of a new magnetic-actuated multi-segment robotic catheter," in *Proc. of 2022 IEEE Int. Conf. on Robotics and Biomimetics (ROBIO)*, pp. 927–932, 2022.

[9] Z. Li and Q. Xu, "Intelligent magnetic control and surgical planning of a multi-segment robotic catheter for endovascular intervention," in *Proc. of 2023 IEEE Int. Conf. on Development and Learning (ICDL)*, pp. 49–54, 2023.

[10] Y. Kim, G. A. Parada, S. Liu, and X. Zhao, "Ferromagnetic soft continuum robots," *Science Robotics*, vol. 4, no. 33, p. eaax7329, 2019.

[11] C. Chautems, S. Lyttle, Q. Boehler, and B. J. Nelson, "Design and evaluation of a steerable magnetic sheath for cardiac ablations," *IEEE Robotics and Automation Letters*, vol. 3, no. 3, pp. 2123–2128, 2018.

[12] C. M. Heunis, K. J. Behrendt, E. E. Hekman, C. Moers, J.-P. P. de Vries, and S. Misra, "Design and evaluation of a magnetic rotablation catheter for arterial stenosis," *IEEE/ASME transactions on mechatronics*, vol. 27, no. 3, pp. 1761–1772, 2021.

[13] A. Ali, D. H. Plettenburg, and P. Breedveld, "Steerable catheters in cardiology: Classifying steerability and assessing future challenges," *IEEE Transactions on Biomedical Engineering*, vol. 63, no. 4, pp. 679–693, 2016.

[14] J. Sikorski, C. M. Heunis, R. Obeid, V. K. Venkiteswaran, and S. Misra, "A flexible catheter system for ultrasound-guided magnetic projectile delivery," *IEEE Transactions on Robotics*, vol. 38, no. 3, pp. 1959–1972, 2022.

[15] M. Waine, C. Rossa, R. Sloboda, N. Usmani, and M. Tavakoli, "3D shape visualization of curved needles in tissue from 2D ultrasound images using ransac," in *Proc. of 2015 IEEE Int. Conf. on Robotics and Automation (ICRA)*, pp. 4723–4728, 2015.

[16] J. C. Norton, P. R. Slawinski, H. S. Lay, J. W. Martin, B. F. Cox, G. Cummins, M. P. Desmulliez, R. E. Clutton, K. L. Obstein, S. Cochran, *et al.*, "Intelligent magnetic manipulation for gastrointestinal ultrasound," *Science Robotics*, vol. 4, no. 31, p. eaav7725, 2019.

[17] W. Wang, J. Qin, L. Zhu, D. Ni, Y.-P. Chui, and P.-A. Heng, "Detection and measurement of fetal abdominal contour in ultrasound images via local phase information and iterative randomized hough transform," *Biomedical Materials and Engineering*, vol. 24, no. 1, pp. 1261–1267, 2014.

[18] M. Barva, M. Uhercik, J.-M. Mari, J. Kybic, J.-R. Duhamel, H. Liebgott, V. Hlavac, and C. Cachard, "Parallel integral projection transform for straight electrode localization in 3-D ultrasound images," *IEEE Transactions on Ultrasonics, Ferroelectrics, and Frequency Control*, vol. 55, no. 7, pp. 1559–1569, 2008.

[19] Z. Yang, L. Yang, M. Zhang, C. Zhang, S. C. H. Yu, and L. Zhang, "Ultrasound-guided catheterization using a driller-tipped guidewire with combined magnetic navigation and drilling motion," *IEEE/ASME Transactions on Mechatronics*, vol. 27, no. 5, pp. 2829–2840, 2022.

[20] J. Stoitsis, S. Golemati, S. Kendros, and K. S. Nikita, "Automated detection of the carotid artery wall in b-mode ultrasound images using active contours initialized by the hough transform," in *Proc. of 2008 30th Annual Int. Conf. of the IEEE Engineering in Medicine and Biology Society*, pp. 3146–3149, 2008.

[21] Z. Li and Q. Xu, "Design and synchronous control of a magnetically-actuated and ultrasound-guided multi-arm robotic system," in *Proc. of 2023 IEEE/RSJ Int. Conf. on Intelligent Robots and Systems (IROS)*, pp. 8425–8430, 2023.

[22] P. Chatelain, A. Krupa, and N. Navab, "Optimization of ultrasound image quality via visual servoing," in *Proc. of 2015 IEEE Int. Conf. on Robotics and Automation (ICRA)*, pp. 5997–6002, 2015.

[23] Z. Li, Z. Li, L. M. Tam, and Q. Xu, "Design and development of a versatile quadruped climbing robot with obstacle-overcoming and manipulation capabilities," *IEEE/ASME Transactions on Mechatronics*, vol. 28, no. 3, pp. 1649–1661, 2023.

[24] R. Castillo-Ortega, N. Marin, C. Martinez-Cruz, and D. Sanchez, "Linguistic comparison of time series using the end-point fit algorithm," in *Proc. of 2015 IEEE Int. Conf. on Fuzzy Systems*, pp. 1–8, 2015.

[25] M. Kaya, A. Denasi, S. Scheggi, E. Agbahca, C. Yoon, D. H. Gracias, and S. Misra, "A multi-rate state observer for visual tracking of magnetic micro-agents using 2D slow medical imaging modalities," in *Proc. of 2018 IEEE/RSJ Int. Conf. on Intelligent Robots and Systems (IROS)*, pp. 1–8, 2018.